

## Molecular dynamics simulation of the rearrangement of polyampholyte conformations on the surface of a charged oblate metal nanospheroid in a microwave electric field

Nikita Yu. Kruchinin<sup>1,a</sup><sup>1</sup>Orenburg State University, Center of Laser and Informational Biophysics, Orenburg, Russia<sup>a</sup>kruchinin\_56@mail.ru

PACS 36.20.-r, 02.70.Ns, 61.46.+w

**ABSTRACT** Using molecular dynamics, the rearrangement of the conformational structure of polyampholytes on the surface of a gold oblate nanospheroid in an alternating electric field was studied depending on the value of its total charge. On the surface of the nanospheroid, at its high total charge and at small amplitude of the alternating electric field strength vector, polyampholyte loops stretched over the entire surface of the nanospheroid. With an increase in the amplitude of the electric field in the equatorial region of the nanospheroid, an annular polyampholytic fringe was formed, ordered by the types of links depending on the distance to the polarization axis of the nanoparticle. In the case of high simulation temperature, the shape of the annular fringe changed twice over a period: in one case, ordering according to the types of links along the polarization axis of the nanospheroid, and in the other case, perpendicular to it.

**KEYWORDS** polyampholyte, oblate metallic nanospheroid, conformational changes, adsorption, molecular dynamics

**ACKNOWLEDGEMENTS** This work was supported by the Ministry of Science and Higher Education of the Russian Federation within the framework of project no. FSGU-2023-0003.

**FOR CITATION** Kruchinin N.Yu. Molecular dynamics simulation of the rearrangement of polyampholyte conformations on the surface of a charged oblate metal nanospheroid in a microwave electric field. *Nanosystems: Phys. Chem. Math.*, 2023, **14** (6), 719–728.

### 1. Introduction

Gold nanoparticles that form conjugates with polymer molecules are widely used in the creation and modification of various chemical sensors based on the effects of surface-enhanced Raman scattering, surface plasmon resonance, and Förster energy transfer between macrochain-bound nanoobjects [1–6]. In addition, such hybrid nanosystems are used for drug delivery, as nanoprobes in biomedicine, and also in other elements of nanoelectronic devices [7–13]. In this case, not only spherical gold nanoparticles can be used, but also ellipsoidal nanoparticles, for example, in the form of elongated and oblate nanospheroids, to obtain nanosystems with adjustable plasmon characteristics [14–17].

One way to control the functional characteristics of such nanosystems is to change the conformational structure of a polyelectrolyte macrochain adsorbed on a nanoparticle under the influence of both an external static electric field and electromagnetic radiation [18–21]. In this case, various functional molecules can be associated with the macrochain, for example, molecules of organic luminophores, as well as small atomic clusters.

In the case of adsorption of polyelectrolyte macromolecules on a charged metal surface, under the influence of electric charges distributed over the metal surface, the conformational structure of the adsorbed macrochain is rearranged. In this case, the conformational changes in the adsorbed polyelectrolyte are affected by the shape of the metal nanoobject and the distribution of the surface density of electric charges on it [22–28]. The conformational structure of a macromolecule adsorbed on a nanoparticle is also significantly affected by the distribution order of charged units in the macrochain. Thus, for generally neutral polyampholyte macromolecules and uniformly charged polyelectrolytes, the character of changes in their conformations during adsorption on the surface of metal nanoparticles charged or polarized in an external electric field is very different [22–28].

When a metal nanoparticle is placed in an external uniform electric field, nonuniformly distributed electric charges are induced on its surface, the surface density of which depends on the shape of the nanoparticle. In this case, the electric field near the surface of the nanoparticle is strongly distorted. The non-uniform distribution of induced electric charges will have a significant effect on the conformational structure of adsorbed polyelectrolytes. For generally neutral polyampholytic polypeptides, as a rule, the extension of macrochain loops along the direction of the induced dipole moment of the metal nanoparticle was observed [22–25].

When a metal nanoparticle is exposed to electromagnetic radiation, the distribution of induced electric charges on the surface of the nanoparticle changes periodically. These temporary changes in the surface charge density lead to a change in the conformational structure of the adsorbed polyelectrolyte macromolecule [29–31]. Previously, conformational changes

in an external alternating electric field of generally neutral polyampholytic polypeptides on the surface of a generally neutral gold nanoparticle of an oblate spheroidal shape were studied [30]. With a periodic change in the polarity of a metal oblate nanospheroid, the links of the polyampholytic macrochain shifted from the poles to the central region and a girdle annular macromolecular fringe was formed, the density and width of which depended on the amplitude of the external polarizing alternating electric field.

A different picture will be observed when a charged metallic oblate nanospheroid with adsorbed polyampholyte is placed in an external alternating electric field. In this case, the electric charges distributed over the surface, due to the presence of a charge in an oblate nanospheroid, will be added to the charges induced by an external electric field. And this will lead to a significant change in the distribution of the surface charge density on the surface of the nanoparticle. Therefore, the conformational structure of a generally neutral polyampholytic macrochain on the surface of a charged oblate nanospheroid in an alternating field will depend on its charge and differ significantly from the previously considered case of a generally neutral oblate nanospheroid [30], as well as from the case of a uniformly charged macrochain [31]. By changing the magnitude and sign of the charge of an oblate metallic nanospheroid, as well as the magnitude of the external alternating electric field, it is possible to control the change in the conformational structure of the adsorbed polyampholyte macrochain.

Thus, the purpose of this work is to study the conformational changes of generally neutral polyampholytic polypeptides on the surface of an oblate charged metal nanospheroid upon changing its polarity at an ultrahigh frequency.

## 2. Molecular dynamics simulation

Molecular dynamics (MD) simulation of polyampholytic polypeptides on the surface of an oblate spheroidal gold nanoparticle was performed using the NAMD 2.14 software package [32], the model of which was obtained by cutting an ellipsoid of rotation from a gold crystal with major semi-axes 3 nm long and minor semi-axes 1.5 nm long. During the simulation, its atoms remained fixed. Four generally neutral polyampholytic polypeptides have been considered:

1) **P1** polypeptide consisting of 402 amino acid residues with 268 Ala (A) units with evenly distributed 67 Asp units (D, charge  $-1e$ ) and 67 Arg units (R, charge  $+1e$ ) –  $(ADA_2RA)_{67}$ ;

2) **P2** polypeptide consisting of 400 amino acid residues with 320 Ala units with evenly distributed 40 Asp units and 40 Arg units –  $(A_2DA_4RA_2)_{40}$ ;

3) **P3** polypeptide consisting of 400 amino acid residues with 320 Ala units with evenly distributed 20 pairs of Asp units and 20 pairs of Arg units –  $(A_4R_2A_8D_2A_4)_{20}$ ;

4) **P4** polypeptide consisting of 412 amino acid residues with 368 Ala units with evenly distributed 11 pairs of Asp units and 11 pairs of Arg units –  $A_8(A_8D_2A_{16}R_2A_8)_{11}A_8$ .

For polypeptides, the CHARMM36 force field was used [33, 34]. The CHARMM all-atom force field is a widely used and well-proven force field for molecular dynamics simulations of proteins, peptides, nucleic acids and lipids. This is a non-reactive force field that includes the following bonded potential energy terms in the potential energy function: valence bonds and angles, torsion angles (dihedrals), impropers, Urey–Bradley, as well as nonbonded potential energy terms: electrostatic Coulombic potential and Lennard–Jones potential. The parameters of the potential energy function terms were determined by fitting an extended set of experimental and ab initio results. The parametrization was based on results for a wide variety of model compounds that represent the protein backbone and the individual side chains. Internal parametrizations (bond length, bond angle, Urey–Bradley, dihedral, and improper dihedral terms) were chosen to reproduce geometries from crystal structures, infrared and Raman spectroscopic data, and ab initio calculations. Interaction parameters (electrostatic and van der Waals terms) were chosen to fit 6–31G\* ab initio interaction energies and geometries for water molecules bonded to polar sites of the model compounds and experimental condensed-phase properties such as heats of vaporization and molecular volumes [33, 34].

Noncovalent interactions with a gold nanospheroid were described by the Lennard–Jones potential parameterized in [35], which is widely used in studying the adsorption of molecules on the surface of gold nanoparticles [36–41]. The van der Waals potential was cut off at a distance of 1.2 nm using a smoothing function between 1.0 and 1.2 nm. Electrostatic interactions were calculated directly at a distance of 1.2 nm, and at a larger distance, the particle mesh Ewald (PME) [42] was used with a grid step of 0.11 nm. The entire nanosystem was placed in a cube with 24 nm edges filled with TIP3P water molecules [43]. Although the TIP3P water model is rigid and coarser compared to many other water models, including the flexible model, the CHARMM force field with this type of water model is well balanced, accurate and computationally efficient, and is therefore widely used in calculations for studying conformational changes of macromolecular chains using the molecular dynamics [44–47].

Polypeptide conformations enveloping an oblate spheroidal nanoparticle (Fig. 1a) obtained as a result of MD simulation on the surface of a neutral nanospheroid in the absence of an external electric field were used as starting points [25]. To obtain the starting conformations, MD simulation was carried out at a constant temperature at 900 K, followed by a decrease to 300 K for a polypeptide macromolecule, which was located in the form of a nonequilibrium coil near the surface of a flattened uncharged and unpolarized nanospheroid. The length of the time trajectory reached 15 ns. This made it possible to achieve deeper conformational minima of the macrochain energy, including on a shorter trajectory section.

To control the obtaining of equilibrium conformations, the change in the root mean square distance between polypeptide atoms in different conformations (RMSD) was monitored [25].

The surface of a spheroidal nanoparticle was charged by assigning partial charges to atoms located on its surface [47, 48]. The distribution of surface charge density on the surface of an oblate metal spheroid charged with a total charge  $Q$  is inhomogeneous [49]:

$$\sigma_Q = \frac{Q}{4\pi a^2 c \sqrt{\frac{x^2+y^2}{a^4} + \frac{z^2}{c^4}}}, \quad (1)$$

Where  $a$  is the length of the major semi-axes, and  $c$  is the length of the minor semi-axis directed along the axis  $z$ , which coincides with the axis of rotation of the spheroid. Gold nanospheroids charged with different total positive charges were considered:  $Q_1 \approx 37.5e$ ,  $Q_2 \approx 75e$  and  $Q_3 \approx 150e$ . At such values of the total charge of an oblate nanospheroid, the atoms that were located on the surface at its poles had partial charges equal to  $+0.025e$ ,  $0+0.05e$ , and  $+0.1e$ , respectively, and the partial charges of atoms located at the equator were 2 times greater (1).

The partial charges on the surface of a charged oblate spheroidal nanoparticle were further summed up with partial charges induced by an external electric field. On the surface of an oblate spheroid polarized in an external uniform electric field directed along the axis of rotation, the surface charge density is distributed according to the formula [49]:

$$\sigma_p = \frac{\sigma_{\max} z}{c^2 \sqrt{\frac{x^2+y^2}{a^4} + \frac{z^2}{c^4}}}, \quad (2)$$

where  $\sigma_{\max} = \frac{p_z}{V}$  is the value of the surface charge density at the pole of an oblate polarized spheroid,  $p_z$  is the dipole moment of the spheroid,  $V$  is the volume of the spheroid.

In the process of modeling, the densities of induced charges periodically changed in time according to the sine law with an oscillation period  $T = 2.4$  ns during 4 oscillation periods. The following peak values of the induced dipole moment of a polarized nanospheroid were considered:  $p_1 \approx 7.7$  and  $p_2 \approx 15.4$  kD. At such values of the dipole moment of an oblate nanospheroid, the atoms on the surface of its positively charged pole had partial charges of  $+0.25e$  and  $+0.5e$ . Each oscillation period was divided into 8 equal time segments of 0.3 ns each, during which the field remained unchanged, and the value of the dipole moment of the nanospheroid on the selected segment was set by averaging it over the entire length of the segment. The dipole moment of the nanoparticle changed in the following sequence, starting from the starting conformation of the polypeptide:  $+0.69p$  (mean value in the range of oscillations from  $\pi/8$  to  $3\pi/8$ ),  $+0.97p$ ,  $+0.69p$ ,  $0$ ,  $-0.69p$ ,  $-0.97p$ ,  $-0.69p$  and  $0$ . The MD simulation was performed at constant temperatures of 300 and 900 K (NVT, Berendsen thermostat). During periodic repolarization of a charged oblate nanospheroid, a narrow belt of atoms appeared in its equatorial region, the charge sign of which did not change and they remained positively charged throughout the entire period (1, 2). To compensate for the excess charge of the entire molecular system, chloride ions were added, which were randomly distributed over the entire simulation cell.

Based on the results of MD simulation, the distributions of the linear density of polypeptide atoms along the axis of rotation of the oblate nanospheroid, as well as the radial distributions of the density of polypeptide atoms in the equatorial region of the nanospheroid, were calculated.

### 3. Results

As a result of MD simulation at a temperature of 300 K of a polyampholyte macrochain on the surface of a neutral oblate metal nanospheroid with a periodic change in time of its polarity at the peak value of the dipole moment  $p_1$ , the amino acid residues of the polypeptide shifted from the vast subpolar regions of the nanoparticle to its narrow equatorial region (Figs. 1b and 1c) [30]. In this case, polyampholyte units were adsorbed on the surface in the vicinity of the equator, regardless of their type. As the peak value of the dipole moment of an oblate nanospheroid increased during modeling with a periodic change in its polarity, the area of strongly charged subpolar regions of the generally neutral nanoparticle increased and, accordingly, the weakly charged equatorial region narrowed (2). Therefore, the narrowing and swelling of the polyampholytic fringe in the equatorial region of the oblate uncharged nanospheroid occurred with a significant ejection of macrochain loops, as well as desorption of some of the links from the surface [30].

A different picture was observed when modeling polyampholytic polypeptides at a temperature of 300 K on the surface of a charged oblate nanospheroid. With an increase in the total charge of an oblate nanospheroid, the force with which negatively charged polyampholyte units are attracted to a positively charged surface increased. Therefore, when modeling with the peak value of the dipole moment  $p_1$  of the nanospheroid, as its total charge increased, the displacement of links from the subpolar regions to the equatorial region became more and more difficult, and at the maximum considered total charge of the nanospheroid, there was almost no displacement of the macrochain to the equator (Figs. 1d,e). On the surface of a strongly charged oblate nanospheroid, at the end of the simulation, with a periodic change in its polarity with a peak value of the dipole moment  $p_1$ , loops were formed over its entire surface from polyampholyte units (Figs. 1d,e) due to the repulsion of like-charged units of the macrochain with respect to the total charge of the nanoparticle.

With an increase in the peak value of the dipole moment of an oblate nanospheroid to  $p_2$ , the absolute value of induced electric charges in the subpolar regions of an oblate nanospheroid increased. Therefore, the charged units of

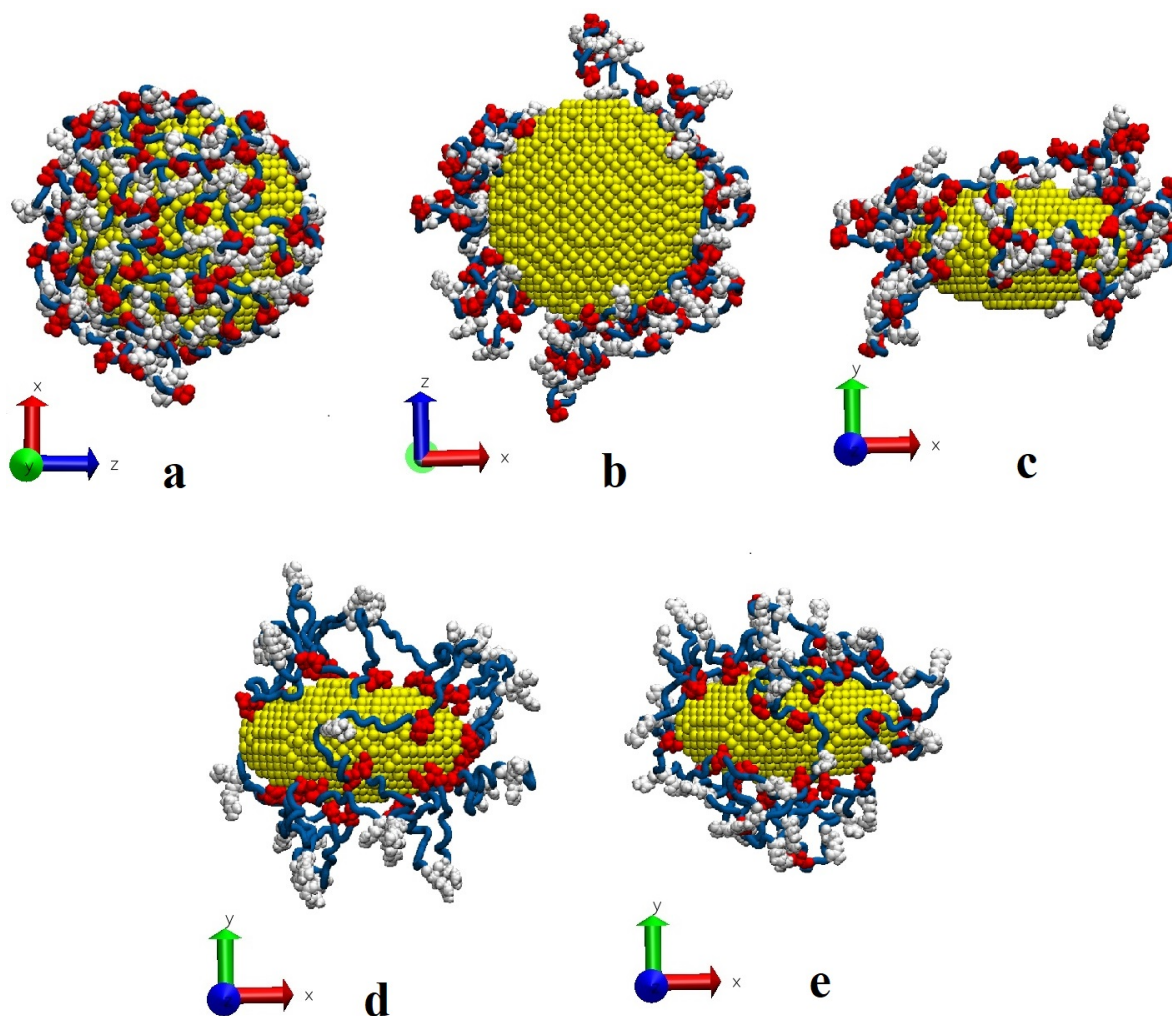


FIG. 1. Starting conformation of polypeptide P1 (a), as well as conformations of polypeptides P1 (b, c), P3 (d) and P2 (e) after MD simulation at a temperature of 300 K with periodic change in polarity on the surface of neutral (b, c) and a charged (d, e) oblate nanospheroid with a total charge  $Q_3$  at the peak value of the dipole moment  $p_1$  (a, b – view along the rotation axis; b, c, d – side view; rotation axis of the nanospheroid and the external electric field are directed along the y axis; blue tube – Ala units, Asp units are shown in red, and Arg units in white)

polyampholyte were pushed out from the similarly charged subpolar regions and gradually, upon repolarization of the oblate nanospheroid, shifted to its equatorial region (Fig. 2), remaining there. This was due to the strong attraction of negatively charged macrochain units to the surface near the equator, in contrast to the case of a neutral oblate spheroidal nanoparticle, where desorption of a large number of macromolecule units was observed [30]. Thus, on the surface of a charged oblate nanospheroid, the ordering of the polyampholytic fringe encircling its edge occurred due to the repulsion of positively charged Arg units from the surface. In this case, the loops of the polyampholyte macrochain were stretched mainly perpendicular to the polarization axis (Fig. 2). It is obvious that when the sign of the total charge of the nanospheroid changes, the order of distribution of concentric layers of charged units of the macrochain in the surrounding annular polyampholytic fringe will change. In this case, on the surface in the equatorial region of the oblate negatively charged nanospheroid there will be a layer of Arg units, and on the periphery, a layer of Asp amino acid residues of the polyampholyte polypeptide.

Figure 3 shows the radial distributions of the atomic density of polyampholytic polypeptides P3 and P1 in the equatorial region of an oblate gold nanospheroid 1 nm wide in the starting conformation (Fig. 3a), as well as at the end of the simulation at a temperature of 300 K with a periodic change in polarity (Fig. 3b,c) of a nanospheroid charged with charge  $Q_3$  at the peak dipole moment  $p_2$ . It can be seen that, in the starting conformation (Fig. 3a), regardless of their type, polyampholyte units are concentrated near the surface of the oblate nanospheroid. In cases where a girdle polyampholyte fringe ordered by unit types was formed in the equatorial region of an oblate spheroidal nanoparticle (at full charge  $Q_3$  and at the peak dipole moment  $p_2$  of an oblate nanospheroid (Fig. 2)), characteristic radial distributions of the density of polyampholyte atoms were formed (Fig. 3b,c). In this case, the profile of the radial distribution of the density of atoms

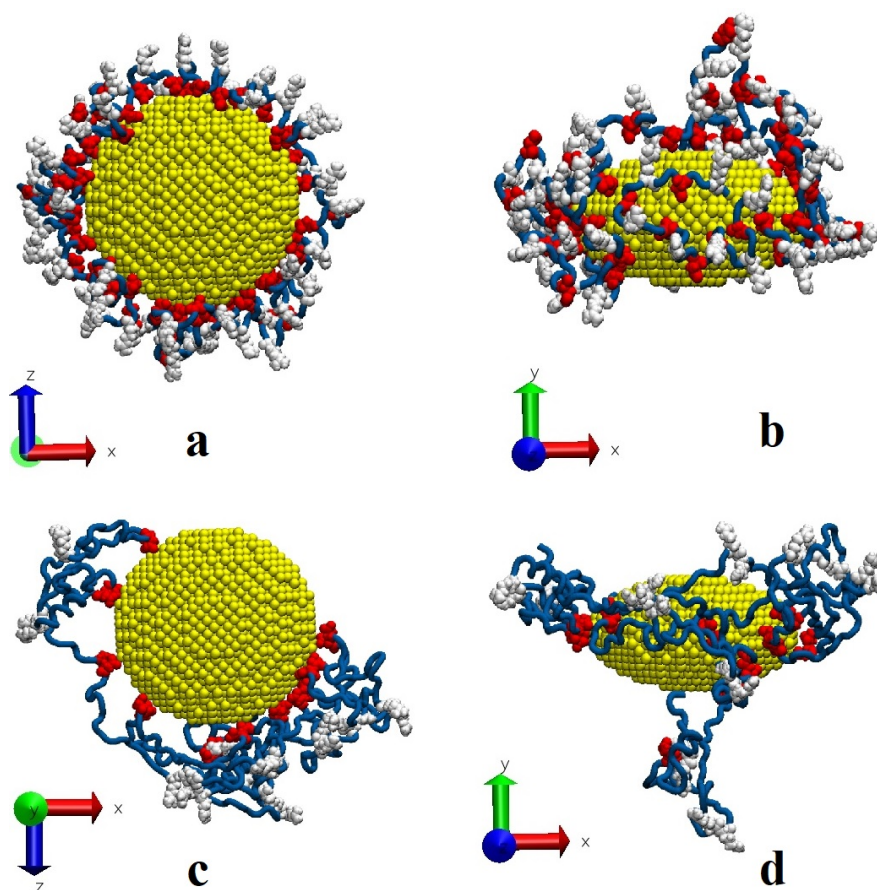


FIG. 2. Conformations of polypeptides P1 (a, b) and P4 (c, d) after MD simulation at a temperature of 300 K with a periodic change in polarity on the surface of an oblate nanospheroid charged with charge  $Q_3$  at the peak value of the dipole moment  $p_2$  (a, c – view along the polarization axis; c, d – side view; rotation axis of the nanospheroid and the external electric field are directed along the  $y$  axis, blue tube – Ala units, Asp units are shown in red, and Arg units in white)

over Asp units, which are charged opposite to the narrow charged equatorial belt of atoms on the surface of the nanoparticle, which do not change the sign of the charge during repolarization, was located closest to the axis of rotation of the nanospheroid. As one moves away from the axis of rotation of the nanospheroid, there is a layer of neutral Ala units, which connect the Arg units repelled from the surface located on the periphery. At the same time, the greater the length of the polypeptide fragment of Ala units, which binds oppositely charged units, the more Arg units moved away from the edge of the oblate nanospheroid in the equatorial region and, thus, the diameter of the formed girdle edge in the transverse direction to the polarization axis increased.

Figure 4 shows the distributions of the linear density of atoms of polyampholytic polypeptides along the axis of rotation of an oblate gold nanospheroid. It can be seen that in the starting conformations (Figs. 4a,b, curves 1) at a distance slightly less than 2 nm on both sides of the beginning of the  $z$  axis, which coincides with the center of the nanospheroid, two characteristic peaks of the linear density of macrochain atoms are observed, corresponding to the adsorption of macrochain units on vast polar regions of the nanospheroid. In the case of modeling at the peak dipole moment  $p_1$  and total charge  $Q_3$  of an oblate nanospheroid, when macrochain loops were ejected over the entire surface of the nanoparticle (Figs. 1c,d), the profile of the linear distribution of the density of polypeptide atoms significantly broadened (Figs. 4a,b, curves 2), and the peaks of these distributions on both sides of the origin of the  $z$  axis were significantly reduced. And at the end of the simulation, at the full charge  $Q_3$  and the peak dipole moment  $p_2$  of the nanospheroid (Figs. 4a,b, curves 3), a single peak was formed on the curves of the linear distribution of the density of polyampholyte atoms at the beginning of the  $z$  axis, which corresponds to the shift of the macrochain links to the equatorial region (Fig. 2).

Figure 5 shows the distributions of the linear density of atoms of the polypeptide P3 along the axis of rotation of the oblate nanospheroid at full charge  $Q_3$  and the peak value of the dipole moment  $p_2$  at the last simulation period for all atoms of the polypeptide (Fig. 5a), as well as for the amino acid residues Arg (Fig. 5b) and Asp (Fig. 5c). It can be seen that at the end of the simulation segments at a temperature of 300 K (Fig. 5, curves 1 and 2), when the dipole moment with the maximum value of the nanospheroid is directed in different directions along the rotation axis, the distribution of the linear density of polypeptide atoms (Fig. 5a, curves 1 and 2) are different from each other. This is due to the displacement

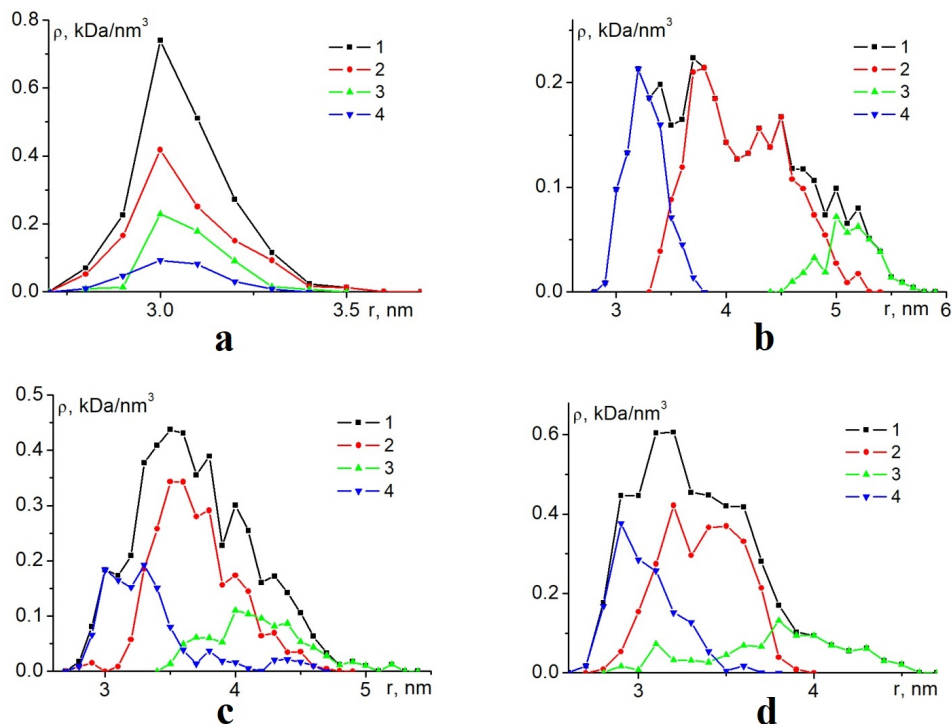


FIG. 3. Radial density distributions of atoms of polypeptides P3 (a, b) and P1 (c, d) in the equatorial region of an oblate gold nanospheroid in the starting conformation (a), as well as at the end of MD simulation at temperatures of 300 K (b, c) and 900 K (d) with a periodic change in the polarity of the nanospheroid charged with charge  $Q_3$  and at the peak dipole moment  $p_2$  (1 – for all atoms of the polypeptide, and 2, 3, and 4 – for amino acid residues Ala, Arg, and Asp)

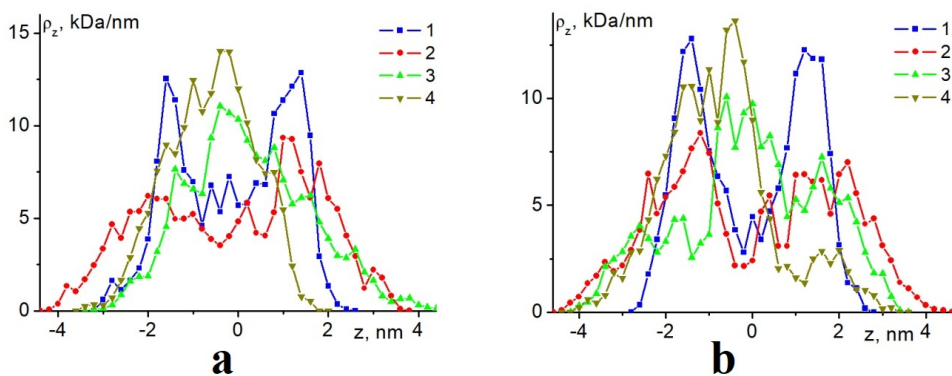


FIG. 4. Linear density distributions of atoms of polypeptides P2 (a) and P3 (b) along the axis of rotation of an oblate gold nanospheroid in the starting conformation (1), as well as at the end of MD simulation at temperatures of 300 K (2, 3) and 900 K (4) as a periodic change in its polarity with a total charge  $Q_3$  at the peak dipole moment  $p_1$  (2) and  $p_2$  (3, 4)

of the charged Arg units (Fig. 5b, curves 1 and 2) from the equatorial region, in contrast to the Asp units, which mostly remained concentrated near the equator (Fig. 5c, curves 1 and 2).

In the MD simulation of polyampholyte polypeptides at a temperature of 900 K on the surface of an oblate gold nanospheroid with a periodic change in its polarity over time, potential barriers that prevent conformational changes in the macrochain were easily overcome, and the conformational structure of the polyampholyte periodically changed following a change in the external electric field. At the end of the simulation segments, when the dipole moment of the nanospheroid was equal to zero, the polyampholyte was concentrated in the narrow equatorial region of the oblate spheroidal nanoparticle (Fig. 6a), as in the simulation with a temperature of 300 K. At the same time, at the maximum considered charge  $Q_3$  of the oblate nanospheroid, as in the simulation with low temperature, the conformational structure of polyampholyte ordered by unit types was formed in the equatorial region (Fig. 6a). For all the considered polypeptides, at the end of the simulation segments, when the dipole moment of the nanospheroid was equal to zero, radial distributions

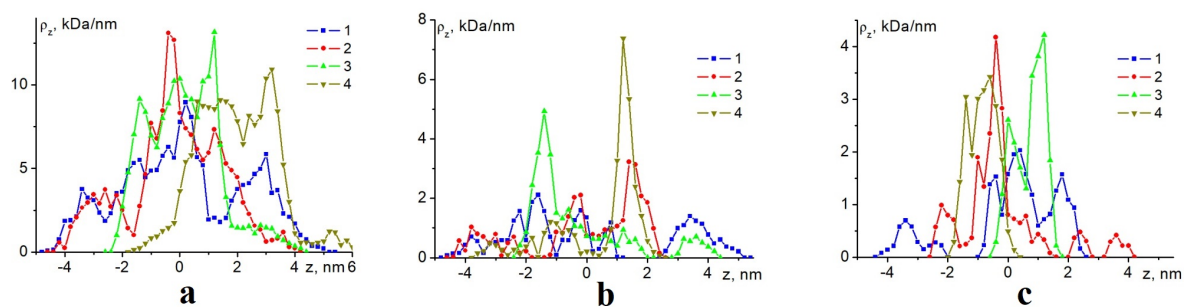


FIG. 5. Linear density distributions of P3 polypeptide atoms along the axis of rotation of an oblate nanospheroid at  $Q_3$  in the last simulation period at temperatures of 300 K (1, 2) and 900 K (3, 4) at the end of time intervals with a peak dipole moment of  $+0.97p_2$  (1, 3) and  $-0.97p_2$  (2, 4) for all atoms of the polypeptide (a), as well as for the amino acid residues Arg (b) and Asp (c)

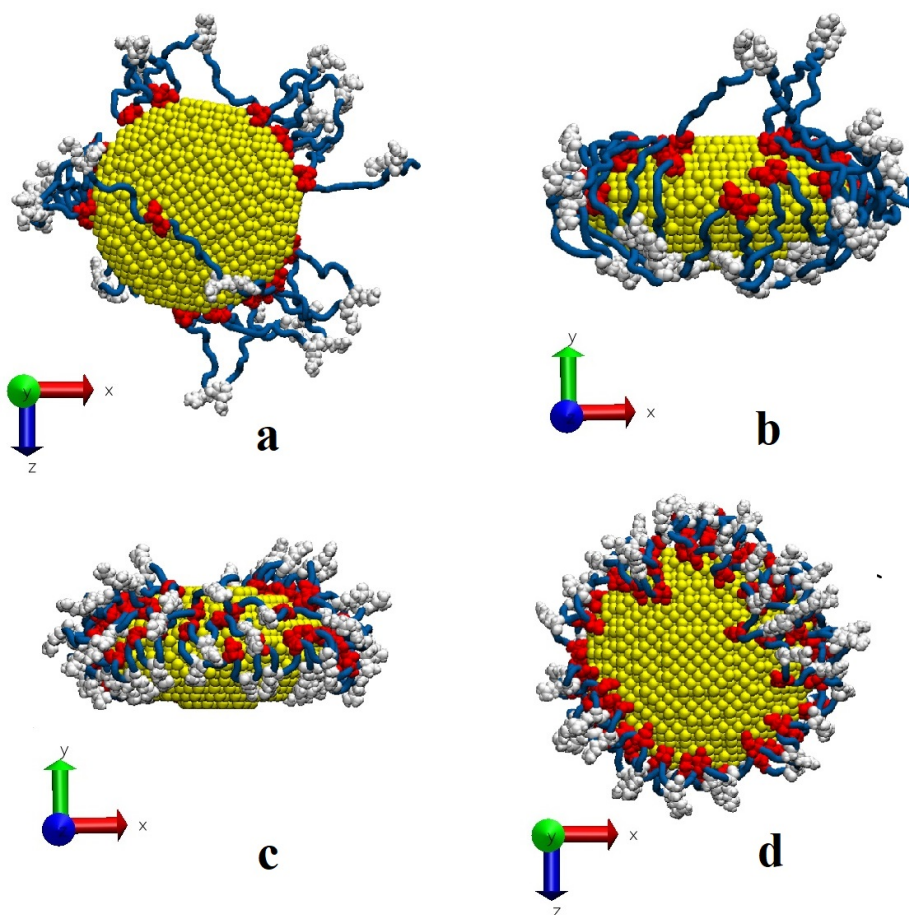


FIG. 6. Conformation of the P3 polypeptide (a) on the surface of an oblate gold nanospheroid at its full charge  $Q_3$  and at the peak dipole moment  $p_2$  at the end of MD simulation with a periodic change in its polarity at a temperature of 900 K (a), as well as the conformations of the P3 polypeptides (b) and P1 (c, d) at the moment of time in the last oscillation period, when the dipole moment has a maximum value (a, d – view along the rotation axis; b, c – side view; rotation axis of the nanospheroid and the external electric field are directed along the y axis; blue tube – Ala units, Asp units are shown in red, and Arg units in white)

of macrochain atomic density similar to those in the case of low temperature were obtained, with differentiation by unit types (Fig. 3d). And on the distributions of the linear density of polypeptide atoms along the axis of rotation of an oblate gold nanospheroid (Fig. 4, curves 4), a peak is observed near the origin of the coordinates of the  $z$  axis, which is much higher than in the simulation with a temperature of 300 K. This is due to the fact that at a higher temperature, the macrochain links are more mobile and they are more easily displaced to the equator and concentrated there.

However, at the end of the MD simulation segments at a temperature of 900 K, when the dipole moment of the oblate charged gold nanospheroid was maximal, in contrast to the case of simulation with a low temperature, the charged units of both Arg and Asp were displaced from the equatorial plane to the edge of oppositely charged polar regions (Fig. 6b,c,d). Moreover, upon repolarization of the nanospheroid, the arrangement of the Arg and Asp units of the polypeptide changed in a mirror manner, and the polar regions of the polarized oblate nanospheroid, as a rule, remained free of adsorbed units of the macrochain (Fig. 6d). As can be seen (Figs. 6b,c,d), at the moments of time when the dipole moment of an oblate nanospheroid is maximum, the conformational structure of the polyampholyte has a clear separation according to the types of units along the rotation axis, encircling the nanoparticle. This is reflected in the distribution curves of the linear density of polypeptide atoms along the axis of rotation of the oblate nanospheroid (Fig. 5, curves 3 and 4). It can be seen that the profiles of linear density distributions over all atoms of the polypeptide (Fig. 5a, curves 3 and 4) at a temperature of 900 K are significantly shifted along the rotation axis for different directions of the dipole moment of the nanoparticle, in contrast to the simulation at a temperature of 300 K (Fig. 5a, curves 1 and 2). The shift of the atomic density profiles along the Arg units at a temperature of 900 K (Fig. 5b, curves 3 and 4) is clearer, and the peaks of these curves are much higher than at low temperature (Fig. 5b, curves 1 and 2). At a low simulation temperature, during polarization reversal of a charged oblate nanospheroid, the profiles of oppositely charged Asp units almost did not shift (Fig. 5c, curves 1 and 2), and at a high temperature, their significant shift relative to the equatorial plane is observed (Fig. 5c, curves 3 and 4).

#### 4. Conclusion

On the surface of a charged oblate gold nanospheroid, when modeling at low temperature with a periodic change in time of its polarity along the axis of rotation at low values of its total charge, as well as at a small amplitude of the polarizing electric field near its equator, a polyampholytic ring-shaped fringe, similar to the case of a generally neutral oblate nanospheroid [30]. As the total charge of the oblate nanospheroid increased and at small amplitude of the polarizing electric field, the macrochain loops stretched over the entire surface of the nanospheroid. At high values of the total charge of an oblate nanospheroid and large amplitude of the polarizing electric field in the equatorial region of the nanospheroid, the annular fringe located perpendicular to the axis of rotation of the nanospheroid was ordered according to the types of polyampholyte units. At the equator, on the surface, there were links of the macrochain, which were charged opposite to the total charge of the nanospheroid. When moving away from the axis of rotation, there was a ring-shaped layer of neutral amino acid residues of the polypeptide. Its thickness in the transverse direction with respect to the polarization axis of the nanospheroid was the greater, the greater was the distance between oppositely charged amino acid residues in the polypeptide. The diameter of the formed girdle ring-shaped macromolecular fringe depended on this distance. On the periphery of the ring-shaped fringe, there was a concentric layer of polyampholyte units, similarly charged with respect to the total charge of the nanospheroid.

When modeling polyampholytic polypeptides on the surface of a charged oblate metal nanospheroid with a periodic change in time of its polarity with high temperature at times when its dipole moment was minimal, the formation of a conformational structure of the adsorbed macrochain was observed, similar to the case of modeling at low temperature. In particular, at the maximum considered total charge of the nanospheroid and the maximum considered amplitude of the polarizing field strength vector at the given time instants, an annular edge ordered by the types of links was formed around the equator of the nanoparticle, depending on the distance to the polarization axis. At other times, when the dipole moment of the nanospheroid was maximal, the annular fringe located near the equator changed its shape and became already ordered along the polarization axis. At the same time, during polarization reversal, the arrangement of oppositely charged links of the macrochain changed in a mirror manner with respect to the equatorial plane. That is, the annular polyampholyte edge changes its shape twice during the period: in one case, ordering according to the types of links along the polarization axis, and in the other case, ordering perpendicular to it.

Thus, in the considered nanosystem, the rearrangement of the macromolecular fringe by the action of an external alternating electric field is possible, depending on the charge of the oblate metal nanospheroid. An annular encircling macromolecular shell with a controlled atomic density is formed on the surface of the nanoparticle. The dielectric properties of such a shell significantly change the characteristics of the polarizability of such a "core-layer" hybrid nanosystem, and the possibility of field modulation of the layer geometry makes it possible to consider it as a control factor for the plasmonic properties of the nanosystem. The macrochain may contain photoactive centers that act as a sensor with light indication. In this case, due to the proximity of the glow center to the surface of the plasmonic nanoparticle, its radiation and kinetic characteristics will have a strong dependence on the distance to the surface, which can be changed under the influence of the electric field of the nanoparticle. Therefore, such a rearrangement of the conformational structure of adsorbed polyampholytes by the action of an external alternating electric, taking into account the charge of an oblate

nanospheroid, can be used to create new and modify existing sensors and nanoprobe based on the effects of surface-enhanced Raman scattering or Förster energy transfer between nanoobjects connected by a macrochain, as well as to create sensitive elements of measuring nanoelectronics and nanomaterials.

## References

- [1] Manikas A.C., Causa F., Moglie R.D., Netti P.A. Tuning gold nanoparticles interfaces by specific peptide interaction for surface enhanced raman spectroscopy (SERS) and separation applications. *ACS Appl. Mater. Interfaces*, 2013, **5**(16), P. 7915–7922.
- [2] Miyazaki C.M., Martin C.S., Constantino C.J.L. Gold conjugated-magnetite nanoparticles for magnetic concentration towards reproducibility and repeatability of SERS measurements. *Colloids and Surfaces A: Physicochemical and Engineering Aspects*, 2023, **671**, P. 131661.
- [3] Qiu M., Zheng S., Li P., Tang L., Xu Q., Weng S. Detection of 1-OHPyr in human urine using SERS with injection under wet liquid-liquid self-assembled films of  $\beta$ -CD-coated gold nanoparticles and deep learning. *Spectrochimica Acta Part A: Molecular and Biomolecular Spectroscopy*, 2023, **290**, P. 122238.
- [4] Zanetti-Polzi L., Charchar P., Yarovsky I., Corni S. Origins of the pH-Responsive photoluminescence of peptide-functionalized Au nanoclusters. *ACS Nano*, 2022, **16**(12), P. 20129–20140.
- [5] Pradhan S.P., Swain S., Sa N., Pilla S.N., Behera A., Sahu P.K., Si S.C. Photocatalysis of environmental organic pollutants and antioxidant activity of flavonoid conjugated gold nanoparticles. *Spectrochimica Acta Part A: Molecular and Biomolecular Spectroscopy*, 2022, **282**, P. 121699.
- [6] Natarajan P., Sukthar P., Changstrom J., Holland C.S., Barry S., Hunter W.B., Sorensen C.M., Tomich J.M. Synthesis and characterization of multifunctional branched amphiphilic peptide bilayer conjugated gold nanoparticles. *ACS Omega*, 2018, **3**(9), P. 11071–11083.
- [7] Wu T., Chen K., Lai W., Zhou H., Wen X., Chan H.F., Li M., Wang H., Tao Y. Bovine serum albumin-gold nanoclusters protein corona stabilized polystyrene nanoparticles as dual-color fluorescent nanoprobe for breast cancer detection. *Biosensors and Bioelectronics*, 2022, **215**, P. 114575.
- [8] Mao M., Xie Z., Ma P., Peng C., Wei X., Liu G. Design and optimizing gold nanoparticle-cDNA nanoprobe for aptamer-based lateral flow assay: Application to rapid detection of acetamiprid. *Biosensors and Bioelectronics*, 2022, **207**, P. 114114.
- [9] Li X., Mao X., Xie W., Liu B., Chen F. Intracellular biosynthesis of gold nanoparticles for monitoring microalgal biomass via surface-enhanced raman spectroscopy. *ACS Sustainable Chem. Eng.*, 2022, **10**(15), P. 4872–4880.
- [10] Zhang H., Wang Z., Wang F., Zhang Y., Wang H., Liu Y. In situ formation of gold nanoparticles decorated  $\text{Ti}_3\text{C}_2$  MXenes nanoprobe for highly sensitive electrogenerated chemiluminescence detection of exosomes and their surface proteins. *Anal. Chem.*, 2020, **92**(7), P. 5546–5553.
- [11] Zhang Y., Tan J., Zhou L., Shan X., Liu J., Ma Y. Synthesis and application of AS1411-functionalized gold nanoparticles for targeted therapy of gastric cancer. *ACS Omega*, 2020, **5**(48), P. 31227–31233.
- [12] Shivashankarappa A., Sanjay K.R., Shah D., Tagat A. Decalepis hamiltonii derived gold nanoparticles and photodynamic cytotoxic evaluation on skin melanoma (B<sub>16</sub>F<sub>10</sub>) cells as an effective drug delivery vehicle. *Journal of Drug Delivery Science and Technology*, 2022, **76**, P. 103766.
- [13] Farhadian N., Kazemi M.S., Baigi F.M., Khalaj M. Molecular dynamics simulation of drug delivery across the cell membrane by applying gold nanoparticle carrier: Flutamide as hydrophobic and glutathione as hydrophilic drugs as the case studies. *Journal of Molecular Graphics and Modelling*, 2022, **116**, P. 108271.
- [14] Rajput P., Shishodia M.S. FRET sensing, and field enhancement near spheroidal nanoparticle: Multipole spectral expansion approach. *Optics Communications*, 2022, **519**, P. 128391.
- [15] Lermé J., Bonnet C., Lebeault M., Pellarin M., Cottancin E. Surface plasmon resonance damping in spheroidal metal particles: quantum confinement, shape, and polarization dependences. *J. Phys. Chem. C*, 2017, **121**(10), P. 5693–5708.
- [16] Pazos-Perez N., de Abajo F.J.G., Fery A., Alvarez-Puebla R.A. From nano to micro: synthesis and optical properties of homogeneous spheroidal gold particles and their superlattices. *Langmuir*, 2012, **28**(24), P. 8909–8914.
- [17] Alsawafta M., Wahbeh M., Truong V. Plasmonic modes and optical properties of gold and silver ellipsoidal nanoparticles by the discrete dipole approximation. *Journal of Nanomaterials*, 2012, **2012**, P. 457968.
- [18] Gomes B.S., Cantini E., Tommasone S., Gibson J.S., Wang X., Zhu Q., Ma J., McGettrick J.D., Watson T.M., Preece J.A., Kirkman-Brown J.C., Publicover S.J., Mendes P.M. On-demand electrical switching of antibody-antigen binding on surfaces. *ACS Appl. Bio Mater.*, 2018, **1**(3), P. 738–747.
- [19] Zhao J., Wang X., Jiang N., Yan T., Kan Z., Mendes P.M., Ma J. Polarization effect and electric potential changes in the stimuli-responsive molecular monolayers under an external electric field. *J. Phys. Chem. C*, 2015, **119**(40), P. 22866–22881.
- [20] Cantini E., Wang X., Koelsch P., Preece J.A., Ma J., Mendes P.M. Electrically responsive surfaces: experimental and theoretical investigations. *Acc. Chem. Res.*, 2016, **49**(6), P. 1223–1231.
- [21] Ghafari A.M., Domínguez S.E., Järvinen V., Gounani Z., Schmit A., Sjöqvist M., Sahlgren C., Salo-Ahen O.M.H., Kvarnström C., Torsi L., Österbacka R. In situ coupled electrochemical-goniometry as a tool to reveal conformational changes of charged peptides. *Advanced Materials Interfaces*, 2022, **9**, P. 2101480.
- [22] Kruchinin N.Yu., Kucherenko M.G. Molecular dynamics simulation of the conformational structure of polyampholyte polypeptides at the surface of a charged gold nanoparticle in external electric field. *Polymer Science Series A*, 2023, **65**(2), P. 224–233.
- [23] Kruchinin N.Yu., Kucherenko M.G. Rearrangements in the conformational structure of polyampholytic polypeptides on the surface of a uniformly charged and polarized nanowire: molecular dynamics simulation. *Surfaces and Interfaces*, 2021, **27**, P. 101517.
- [24] Kruchinin N.Yu., Kucherenko M.G. Molecular dynamics simulation of conformational rearrangements in polyelectrolyte macromolecules on the surface of a charged or polarized prolate spheroidal metal nanoparticle. *Colloid Journal*, 2021, **83**(5), P. 591–604.
- [25] Kruchinin N.Yu., Kucherenko M.G. Statistical and molecular-dynamics simulation of electrically induced changes in the conformational structure of polyampholytes on the surface of a flattened metal nanospheroid. *Colloid Journal*, 2022, **84**(2), P. 169–182.
- [26] Kucherenko M.G., Kruchinin N.Yu., Neyasov P.P. Modeling of conformational changes of polyelectrolytes on the surface of a transversely polarized metal nanowire in an external electric field. *Eurasian Physical Technical Journal*, 2022, **19**(2), P. 19–29.
- [27] Kruchinin N.Yu., Kucherenko M.G. Molecular dynamics simulation of the conformational structure of uniform polypeptides on the surface of a polarized metal prolate nanospheroid with varying pH. *Russian Journal of Physical Chemistry A*, 2022, **96**(3), P. 624–632.
- [28] Kruchinin N.Yu., Kucherenko M.G., Neyasov P.P. Modeling conformational changes in uniformly charged polyelectrolytes on the surface of a polarized metallic oblate nanospheroid. *Russian Journal of Physical Chemistry A*, 2022, **96**(12), P. 2718–2728.
- [29] Kruchinin N.Yu., Kucherenko M.G. Modeling the conformational rearrangement of polyampholytes on the surface of a prolate spheroidal metal nanoparticle in alternating electric field. *High Energy Chemistry*, 2021, **55**(6), P. 442–453.
- [30] Kruchinin N.Yu., Kucherenko M.G. Conformational changes in polyampholyte macrochains on the surface of an oblate metallic nanospheroid in alternating electric field. *High Energy Chemistry*, 2022, **56**(6), P. 499–510.

- [31] Kruchinin N.Yu., Kucherenko M.G. Rearrangements in the conformational structure of polyelectrolytes on the surface of a flattened metal nanospheroid in an alternating electric field. *Colloid Journal*, 2023, **85**(1), P. 44–58.
- [32] Phillips J.C., Braun R., Wang W., Gumbart J., Tajkhorshid E., Villa E., Chipot C., Skeel R.D., Kalé L., Schulten K. Scalable molecular dynamics with NAMD. *J Comput Chem.*, 2005, **26**, P. 1781–1802.
- [33] MacKerell Jr. A.D., Bashford D., Bellott M., Dunbrack Jr. R.L., Evanseck J.D., Field M.J., Fischer S., Gao J., Guo H., Ha S., Joseph-McCarthy D., Kuchnir L., Kuczera K., Lau F.T.K., Mattos C., Michnick S., Ngo T., Nguyen D.T., Prodhom B., Reiher W.E., Roux B., Schlenkrich M., Smith J.C., Stote R., Straub J., Watanabe M., Wiórkiewicz-Kuczera J., Yin D., Karplus M. All-atom empirical potential for molecular modeling and dynamics studies of proteins. *J. Phys. Chem. B.*, 1998, **102**(18), P. 3586–3616.
- [34] Huang J., Rauscher S., Nawrocki G., Ran T., Feig M., de Groot B.L., Grubmüller H., MacKerell Jr. A.D. CHARMM36m: an improved force field for folded and intrinsically dis-ordered proteins. *Nature Methods*, 2016, **14**, P. 71–73.
- [35] Heinz H., Vaia R.A., Farmer B.L., Naik R.R. Accurate simulation of surfaces and interfaces of face-centered cubic metals using 12–6 and 9–6 Lennard-Jones potentials. *J. Phys. Chem. C*, 2008, **112**(44), P. 17281–17290.
- [36] Jia H., Zhang Y., Zhang C., Ouyang M., Du S. Ligand-ligand-interaction-dominated self-assembly of gold nanoparticles at the oil/water interface: an atomic-scale simulation. *J. Phys. Chem. B*, 2023, **127**(10), P. 2258–2266.
- [37] Cappabianca R., De Angelis P., Cardellini A., Chiavazzo E., Asinari P. Assembling biocompatible polymers on gold nanoparticles: toward a rational design of particle shape by molecular dynamics. *ACS Omega*, 2022, **7**(46), P. 42292–42303.
- [38] Xiong Q., Lee O., Mirkin C.A., Schatz G. Ethanol-induced condensation and decondensation in DNA-linked nanoparticles: a nucleosome-like model for the condensed state. *Journal of the American Chemical Society*, 2023, **145**(1), P. 706–716.
- [39] Wei X., Harazinska E., Zhao Y., Zhuang Y., Hernandez R. Thermal transport through polymer-linked gold nanoparticles. *The Journal of Physical Chemistry C*, 2022, **126**(43), P. 18511–18519.
- [40] Yokoyama K., Thomas J., Ardner W., Kieft M., Neuwirth L.S., Liu W. An approach for in-situ detection of gold colloid aggregates amyloid formations within the hippocampus of the Cohen's Alzheimer's disease rat model by surface enhanced raman scattering methods. *Journal of Neuroscience Methods*, 2023, **393**, P. 109892.
- [41] Wang X., Ham S., Zhou W., Qiao R. Adsorption of rhodamine 6G and choline on gold electrodes: a molecular dynamics study. *Nanotechnology*, 2023, **34**, P. 025501.
- [42] Darden T., York D., Pedersen L. Particle mesh Ewald: An N-log(N) method for Ewald sums in large systems. *J. Chem. Phys.*, 1993, **98**, P. 10089–10092.
- [43] Jorgensen W.L., Chandrasekhar J., Madura J.D., Impey R.W., Klein M.L. Comparison of simple potential functions for simulating liquid water. *J. Chem. Phys.*, 1983, **79**, P. 926–935.
- [44] Chen Y., Cruz-Chu E.R., Woodard J.C., Gartia M.R., Schulten K., Liu L. Electrically induced conformational change of peptides on metallic nanosurfaces. *ACS Nano*, 2012, **6**, P. 8847–8856.
- [45] Mahinthichaichan P., Tsai C., Payne G.F., Shen J. Polyelectrolyte in electric field: disparate conformational behavior along an aminopolysaccharide chain. *ACS Omega*, 2020, **5**, P. 12016–12026.
- [46] Si W., Yu M., Wu G., Chen C., Sha J., Zhang Y., Chen Y. A nanoparticle-DNA assembled nanorobot powered by charge-tunable quad-nanopore system. *ACS Nano*, 2020, **14**, P. 15349–15360.
- [47] Shankla M., Aksimentiev A. Conformational transitions and stop-and-go nanopore transport of single-stranded DNA on charged grapheme. *Nature Communications*, 2014, **5**, P. 5171.
- [48] Chen P., Zhang Z., Gu N., Ji M. Effect of the surface charge density of nanoparticles on their translocation across pulmonary surfactant monolayer: a molecular dynamics simulation. *Molecular Simulation*, 2018, **44**, P. 85–93.
- [49] Landau L.D., Pitaevskii L.P., Lifshitz E.M. *Electrodynamics of Continuous Media*, 2nd Edition, Elsevier Ltd., 1984, 460 p.

---

Submitted 8 September 2023; revised 30 October 2023; accepted 5 November 2023

*Information about the authors:*

Nikita Yu. Kruchinin – Orenburg State University, Center of Laser and Informational Biophysics, Orenburg, Russia;  
ORCID 0000-0002-7960-3482; kruchinin\_56@mail.ru